ISSN1346－7832

独立行政法人港湾空港技術研究所

港湾空港技術研究所報告

REPORT OF THE PORT AND AIRPORT RESEARCH INSTITUTE

VOL.45 NO.4 December 2006

NAGASE, YOKOSUKA, JAPAN

INDEPENDENT ADMINISTRATIVE INSTITUTION,
PORT AND AIRPORT RESEARCH INSTITUTE

港湾空港技術研究所報告（REPORT OF PARI）
第45巻　第4号　(Vol.45, No.4),　2006年12月(December 2006)

目　　次（CONTENTS）

1．波崎海洋研究施設で観測された沿岸砂州の中・長期変動特性およびその影響要因
……栗山　善昭・柳嶋　慎一 …… 1
(Medium-Term Variations of Bar Properties and Their Linkages with Environmental Factors at HORS
…… Yoshiaki KURIYAMA, Shin-ichi YANAGISHIMA)

2．波崎海洋研究施設で取得された長期現地観測データに基づく卓越沿岸流の岸沖分布の検討
……栗山　善昭・柳嶋　慎一 …… 15
(Cross-shore Variation of Long-Term Average Longshore Current Velocity at HORS
…… Yoshiaki KURIYAMA, Shin-ichi YANAGISHIMA)

3．有機スズ化合物の港湾堆積物への吸着特性に関する実験
……中村　由行・山崎　智弘・小沼　晋・加賀山　亨・益永　茂樹 …… 31
(Adsorption Characteristics of Organotin Compounds onto Ports and Harbors Sediments
……Yoshiyuki NAKAMURA,
Tomohiro YAMASAKI, Susumu KONUMA, Akira KAGAYAMA, Shigeki MASUNAGA)

4．砂質干潟の生態土砂環境場に果たすサクションの役割
－巣穴住活動／保水場の性能評価・設計指針－
……佐々　真志・渡部　要一 …… 61
(The Role of Suction in Tidal Flat Geoenvironments and Burrowing Activity of Benthos
-Performance Index for Conservation and Restoration of Intertidal Sandy Flats-
……Shinji SASSA, Yoichi WATABE)

REPORT OF THE PORT AND
AIRPORT RESEARCH INSTITUTE
Vol.45,No.4(Dec.2006)

Cross-shore Variation of Long-Term Average Longshore Current Velocity at HORS

Yoshiaki KURIYAMA*
Shin-ichi YANAGISHIMA**

Synopsis

The cross-shore variation of long-term average longshore current velocity was investigated on the basis of a 15-year data set of longshore current, wave and wind. The longshore current velocities were measured once a day along a 427-meter-long pier. The results show that the direction of the long-term average longshore current velocity away (> 200 m) from the shore was opposite to that near the shore. The southward current was dominant offshore, whereas the northward current was dominant near the shore. The cross-shore variation of the long-term average longshore current velocity was formed owing to a difference between the wave and wind conditions when the northward and southward currents developed. When the northward current developed, the deepwater wave height was relatively small and the frequency of the wind from the north was almost equal to that from the south. As a result, the northward current developed only near the shore and decayed outside the narrow surf zone. On the other hand, when the southward current developed, the deepwater wave height was relatively large and the wind from the north was predominant, which resulted in the southward current developing not only in the wide surf zone but also outside the surf zone. The superposition of the two cross-shore variations produced the cross-shore variation of the long-term average longshore current velocity with a northward velocity near the shore and a southward velocity away from the shore.

Key Words: longshore current, surf zone, nearshore zone, wave, wind

* Head, Littoral Drift Division, Marine Environment and Engineering Department
** Senior Research Engineer, Marine Environment and Engineering Department
Nagase 3-1-1, Yokosuka, Kanagawa 239-0826, Japan
Phone：+81-46-844-5045 Fax：+81-46-841-9812 e-mail: kuriyama@pari.go.jp

港湾空港技術研究所報告
第 45 巻第 4 号(2006.12)

波崎海洋研究施設で取得された長期現地観測データに基づく卓越沿岸流の岸沖分布の検討

栗山　善昭*・柳嶋　慎一**

要　　旨

茨城県波崎海岸において 15 年間にわたり 1 日 1 回ほぼ毎日取得した沿岸流速データを解析した．卓越沿岸流の方向は岸と沖で異なっており，岸側では北向きの沿岸流が卓越したのに対して，沖側では南向きの沿岸流が卓越した．この原因は，北向きの沿岸流が生じた場合には，波高が相対的に小さく，北から及び南からの風が同じ頻度であったのに対して，南向きの沿岸流が生じた場合には，波高が大きく，北からの風が卓越していたことにある．前者では，汀線近傍の狭い砕波帯内のみで北向き沿岸流が発達するのに対して，後者では，砕波帯幅が広く，砕波帯外でも風による沿岸流が発達するため岸沖方向に一様に近い南向き沿岸流が形成される．以上の流速分布が重なり，卓越沿岸流の向きが岸と沖で異なった．

キーワード：沿岸流，砕波帯，沿岸域，波，風

* 海洋・水工部　漂砂研究室長
** 海洋・水工部　主任研究官
〒239-0826　横須賀市長瀬3-1-1　独立行政法人　港湾空港技術研究所
電話：046-844-5045　Fax：046-841-9812　　e-mail: kuriyama@pari.go.jp

CONTENTS

Synopsis ····· 15

1. Introduction ····· 19

2. Field measurements ····· 19

3. Results ····· 21
3.1 Cross-shore variation of long-term average longshore current velocity ····· 21
3.2 Cross-shore gradient of radiation stress and wind stress ····· 23
3.3 Causes of cross-shore variation of long-term average longshore current ····· 25

4. Discussion ····· 26

5. Conclusions ····· 28

Acknowledgements ····· 28

References ····· 29

1. Introduction

Longshore currents in the nearshore zone induced by obliquely incident waves and winds transport sediments alongshore, and longshore current velocities averaged for long-term periods cause long-term morphological changes. Hence, understanding the long-term average longshore current velocity is essential for sediment budget analysis and for effective coastal zone management.

The cross-shore variation of the longshore current velocity has been investigated since the 1940s [*Horikawa*, 1978]. A number of measurements have been conducted in the field and in laboratories [e.g., *Thornton and Guza*, 1986; *Visser*, 1984; *Smith et al.*, 1993; *Kuriyama and Ozaki*, 1993; *Reniers and Battjes*, 1997; *Garcez-Faria et al.*, 1998; *Ruessink et al.*, 2001; *Hamilton and Ebersole*, 2001], and many one-dimensional models have been developed [e.g., *Longuet-Higgins*, 1970a, b; *Thornton and Guza*, 1986; *Larson and Kraus*, 1991; *Goda and Watanabe*, 1991; *Smith et al.*, 1993; *Church and Thornton*, 1993; *Kuriyama and Nakatsukasa*, 2000; *Ruessink et al.*, 2001]. Studies on longshore current have been reviewed by *Horikawa* [1978] and *Komar* [1998]. Using one of the models, *Ruessink et al.* [2001] predicted temporal variations of longshore current velocities corresponding to the changes in waves, winds, tides and bathymetries for relatively short-term periods, one to two months, and showed that the predicted values agreed well with the measured values.

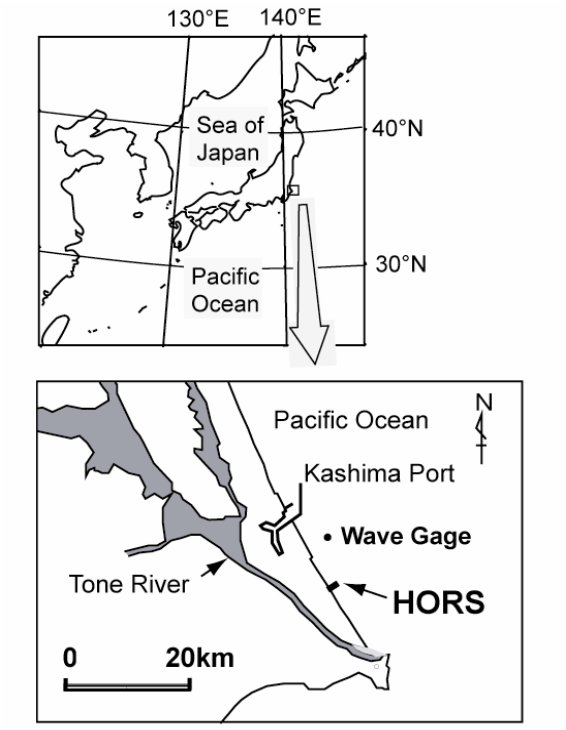

Figure 1 Locations of the study site and offshore wave gage.

The direction of the long-term average longshore current velocity near the shore can be detected from the long-term shoreline change around a coastal structure because the long-term average longshore current velocity induces accumulation on the updrift side of a coastal structure and erosion on the downdrift side [e.g., *Komar*, 1998]. However, because of the lack of field data and numerical simulation results of longshore current velocities away from the shore over long-term periods, the cross-shore variation of the long-term average longshore current velocity is poorly understood, although Sato [1996] suggested that the direction of the long-term average longshore current velocity offshore may be the opposite to that near the shore.

The objective of this study was to investigate the cross-shore variation of the long-term average longshore current velocity on the basis of a 15-year data set of longshore current velocities measured in the nearshore zone on a dissipative beach.

2. Field measurements

Field measurements of longshore current velocity were conducted once a day from 1987 to 2001 at intervals of about 50 m along a 427-meter-long pier of the Hazaki Oceanographical Research Station (HORS), located on the Hasaki Coast of Japan facing the Pacific Ocean (**Figure 1**).

Nearshore current velocities 1 m below the water surface were measured with a spherical float having a diameter of 0.2 m (**Figure 2**); the density of the float was slightly greater than that of seawater. The float was connected with an identification buoy by a 1-meter-long rope. The length of the rope was shortened as necessary when the mean water depth was small.

The float attached to a 30-m-long line was released from the pier, and the time for full extension of the line was measured with a stopwatch (**Figure 2**). The current velocity was calculated from the time and the length of the line. The transport direction of the float due to the nearshore current

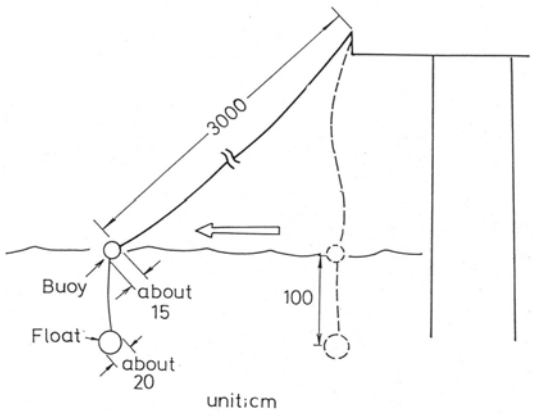

Figure 2 Float for the measurement of longshore current velocity.

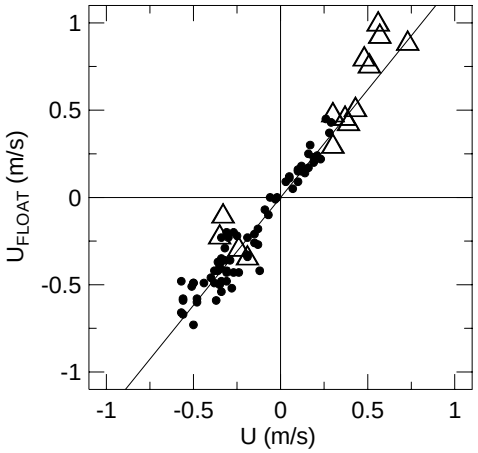

Figure 3 Relationship between the longshore current velocities measured with the electro-magnetic current meter U and those with the float U_{FLOAT}. The open triangles represent the data obtained when the absolute value of the wind velocity exceeded 8 m/s.

was observed with a protractor. At each measurement point, currents were measured three times and the averaged value was used for the analysis. It took about 60 minutes to measure the nearshore currents along the pier.

The validity of this measurement method was confirmed with longshore current velocities 1 m below the water surface simultaneously measured with the present method and an electromagnetic current meter [*Kuriyama and Ozaki*, 1993; *Kuriyama*, 1995]. The relationship between the time-averaged longshore current velocities measured with the float U_{FLOAT} and those measured with the current meter U (**Figure 3**) showed a very strong correlation between them, with only a small influence of the wind. The correlation coefficient r was

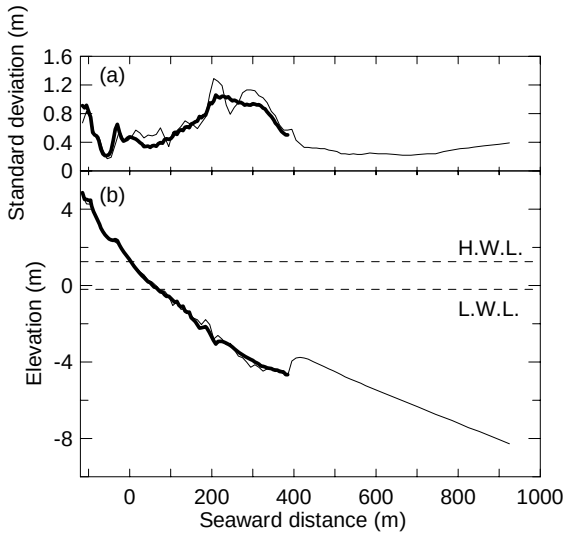

Figure 4 Standard deviations in elevation (a) and the mean beach profiles (b) based on the daily profile measurements along the HORS pier (thick lines) and yearly bathymetry surveys around HORS (thin lines) (Kuriyama, 2002). The elevation is based on the Hasaki datum level.

0.97, and the standard deviation was 0.086 m/s. The relationship between them was expressed as

$$U = 0.81 U_{FLOAT}\,. \qquad (1)$$

In the following analysis, the values of U are used.

The measurement points were located where the seaward distance was 115, 145, 190, 245, 280, 330 and 380 m. Each position along the pier is referred to as the seaward distance relative to the reference point, located close to the entrance of the pier and designated as "P." For example, P115m denotes a position 115 m seaward from the reference point.

Because the locations of the measurement points during the period from January 1987 to June 1988 were different from those mentioned above, the longshore current velocities at the normal measurement points during the period were interpolated with the values measured at different locations by using a third order spline function.

The averaged beach profiles show that the beach slope during the measurement period decreased gradually in the offshore direction (**Figure 4**). It was about 1/40 near the shoreline, about 1/100 at P300m and about 1/120 seaward of the tip of the pier. In the region between P200m and P400m, longshore bars emerged, migrated seaward and decayed.

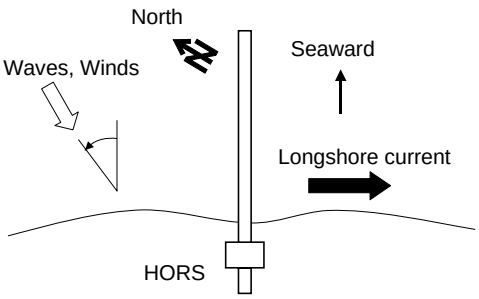

Figure 5 The coordinate system at HORS.

Although local scours were observed in trough regions and the discontinuity of the averaged beach profile at P400m was probably caused by these local scours, the locations and elevations of bar crests and the locations of toughs were almost uniform alongshore [*Kuriyama*, 2002].

Besides the longshore current velocities, the wave angle was visually observed at the tip of the pier. At P380m and P145m, waves were measured with ultrasonic wave gages at a sampling interval of 0.3 s for 20 minutes every hour. Wind angle and velocity were measured at the tip of the pier for 10 minutes every hour. Deepwater waves were measured at a water depth of about 24 m with an ultrasonic wave gage for 20 minutes every 2 hours (**Figure 1**). The wave heights and periods during the period of 25 days from February 7 to March 3, 1993, for which data were missing, were estimated using the method of *Hashimoto et al.* [2000].

The positive direction for the longshore current velocity was defined as being southward (Figure 5). The wave and wind angles were defined relative to the shoreward direction and were positive in the counterclockwise one.

The seasonal change of the deepwater wave height was large from January to March and from September to October, but small from June to August (**Figure 6 (a)**). On the other hand, the wave period was almost constant at 8 s (b). Waves mainly came from the north in December to February, and from the south in May to August (c). Strong winds came from the north in October to February, whereas weak winds came from the south in May to August (d). Compared with the seasonal changes, yearly changes were relatively small (**Figure 7**).

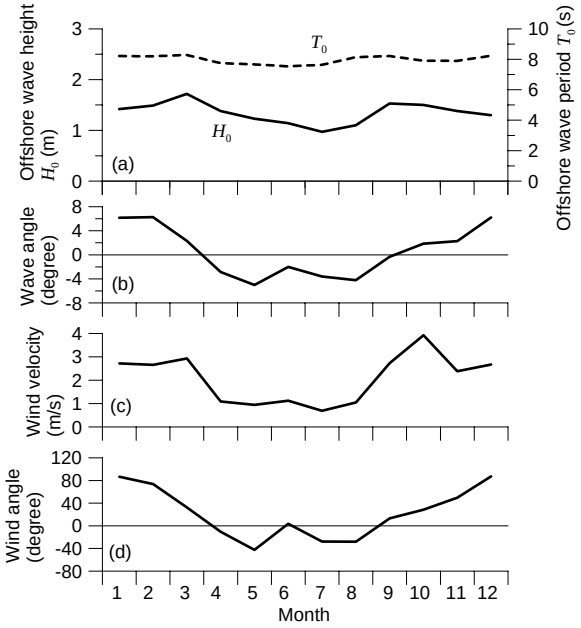

Figure 6 Monthly average offshore wave height and period, wave angle visually observed at the tip of the HORS pier, and wind velocity and angle.

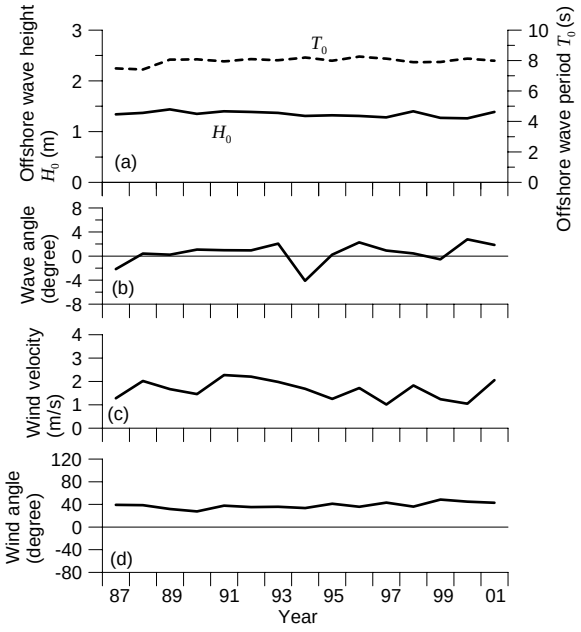

Figure 7 Yearly average offshore wave height and period, wave angle visually observed at the tip of the HORS pier, and wind velocity and angle.

3. Results

3.1 Cross-shore variation of long-term average longshore current velocity

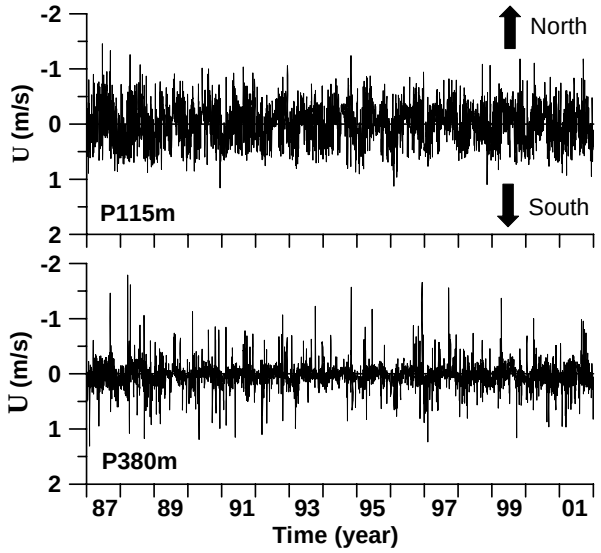

Figure 8 Time-series of longshore current velocities measured at P115m and P380m.

The time series of the measured longshore current velocities are shown in **Figure 8**. **Figure 9** shows those of the cumulative longshore current velocities U_{cuml}, which are expressed as Eq. (2), and the cross-shore variation of the cumulative longshore current velocity at the end of the measurement period, which is proportional to the longshore current velocity averaged in the long term, 15 years.

$$U_{culm} = \Sigma U \Delta t, \qquad (2)$$

where Δt is the time interval.

Figure 9 demonstrates that the direction of the long-term average longshore current velocity varies in the measurement area; it was northward shoreward of P150m, but southward seaward of P200m.

Because the cross-shore variation shown in Figure 9 is formed by the difference between the cross-shore variations of the northward and southward longshore current velocities, the cumulative longshore current velocities and the time-averaged longshore current velocities when the velocity direction at P115m was northward and southward were estimated; the frequencies of the northward and southward longshore currents at P115m were 2,924 and 2,549, respectively. When the northward current developed at P115m, the absolute value of the time-averaged longshore current velocity decreased seaward (Figure 10). On the other hand, when the southward current developed, although the absolute value of the velocity also decreased seaward, the amount of the decrease was smaller than that with the northward current. The frequency of the northward current was larger than that of the southward current, and as a result, the northward

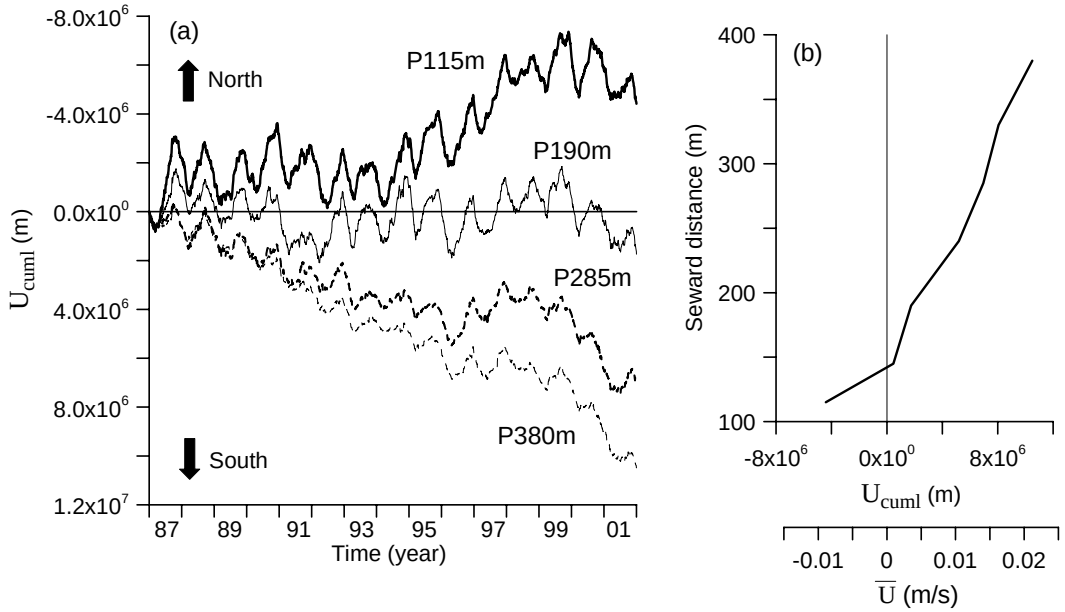

Figure 9 (a) Time-series of cumulative longshore current velocities U_{cuml} at P115m, P190m, P285m and P380m. (b) Cross-shore variation of cumulative longshore current velocity U_{cuml} at the end of the measurements and the long-term average longshore current velocity $\overline{U}$.

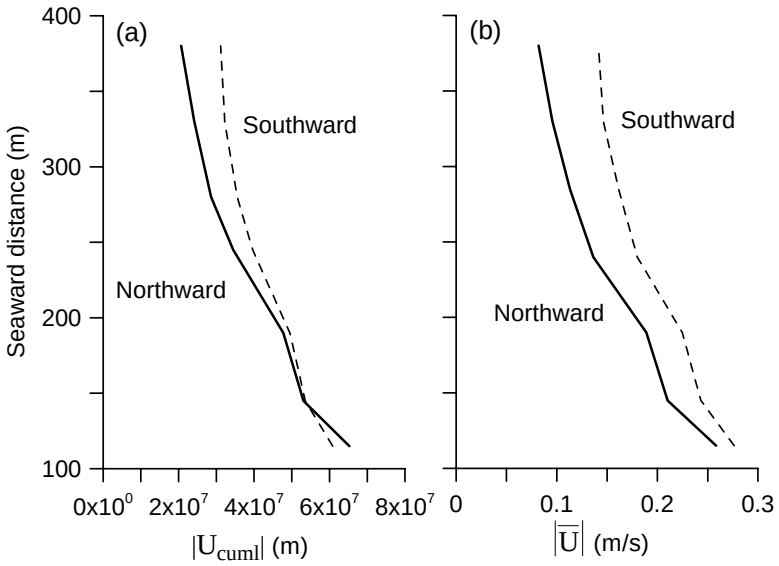

Figure 10 Cross-shore distributions of the absolute values of the longshore current velocities when the longshore current direction at P115m was northward (solid line) and southward (broken line). (a) Cumulative longshore current velocity at the end of the measurement period, and (b) long-term average longshore current velocity.

longshore current was predominant near the shore, whereas the southward current was predominant away from the shore (**Figure 9**).

3.2 Cross-shore gradient of radiation stress and wind stress

The longshore current in the nearshore zone is generated mainly by waves and winds. In order to investigate the causes of the cross-shore variation of the long-term average longshore current velocity, the contributions of the waves and winds to the long-term average longshore current velocity were estimated on the basis of a momentum balance equation for longshore current velocity.

The momentum balance equation usually includes the cross-shore gradient of radiation stress, wind stress and lateral mixing term. However, because the influence of the lateral mixing term on the longshore current velocity under irregular waves is small [*Thornton and Guza*, 1986; *Goda and Watanabe*, 1991], the momentum balance equation without the lateral mixing term (Eq. (3)) was used.

$$\tau_b - dS_{yx}/dy - \tau_s = 0, \tag{3}$$

where τ_b is the bottom friction stress, S_{yx} is the radiation stress, y is the seaward distance, and τ_s is the wind stress.

Although estimation of the radiation stress requires accurate measurement of wave angle, these angles were not accurately measured. Hence, the gradient of the radiation stress was estimated from the bottom friction stress and the wind stress with Eq. (3).

The bottom friction stress was estimated with a nonlinear formula [*Nishimura*, 1988] expressed as

$$\tau_b = C_f \rho_w \sqrt{U^2 + w_b^2}\, U, \qquad w_b = 2\nu_m / \pi, \quad \nu_m = \pi H / \left[T \sinh(2\pi h / L)\right], \tag{4}$$

where C_f is a nondimensional coefficient, ρ_w is the sea water density, v_m is the amplitude of the orbital velocity at the bottom. The formula has been used by *Larson and Kraus* [1991] and *Kuriyama and Nakatsukasa* [2000]. The wave angle, included in the original formula of *Nishimura* [1988], was assumed to be zero owing to the lack of accurate wave angle data. The significant wave heights $H_{1/3}$ were used as the wave height for the estimation of v_m, and $H_{1/3}$ values along the pier were estimated from the deepwater wave heights and periods using a 1-D wave transformation model for irregular waves evaluated with field data obtained at the study site [*Kuriyama and Nakatsukasa*, 2000]. Wave refraction was not considered in the estimation. The beach profiles measured daily were used for the profile shoreward of P385m, while the

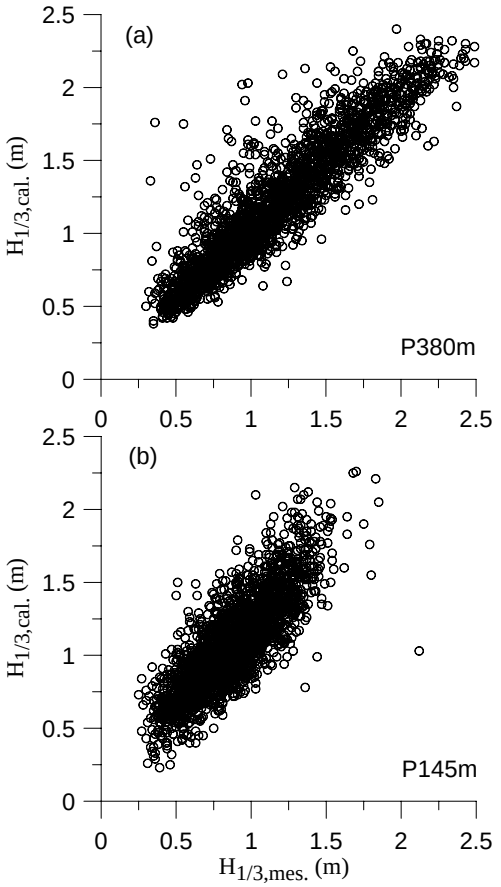

Figure 11 Comparisons between the measured and predicted $H_{1/3}$ at P380m (a) and P145m (b).

averaged beach profile was used for that seaward of P445m. The beach profiles between P385m and P445m were linearly interpolated with the elevations at P385m and P445m. The grid interval was 10 m, and the seaward boundary was set at P925m, where the elevation of the beach profile is -8.28 m and waves seldom break.

The model was verified with significant wave heights measured at P380m and P145m (**Figure 11**). The model values agreed with the measured ones although the model slightly overestimated the wave height at P145m. The overall root-mean-square error ε defined as Eq. (5) is 30%.

$$\varepsilon = \sqrt{\sum (H_{mes.} - H_{pred.})^2 \Big/ \sum H_{mes.}^2} \qquad (5)$$

where $H_{mes.}$ and $H_{pred.}$ are the significant wave heights measured and predicted, respectively.

The coefficient of the bottom friction stress was set at 0.005 as in *Kuriyama and Nakatsukasa* [2000]. The value of 0.005 is close to the value obtained for the coefficient of

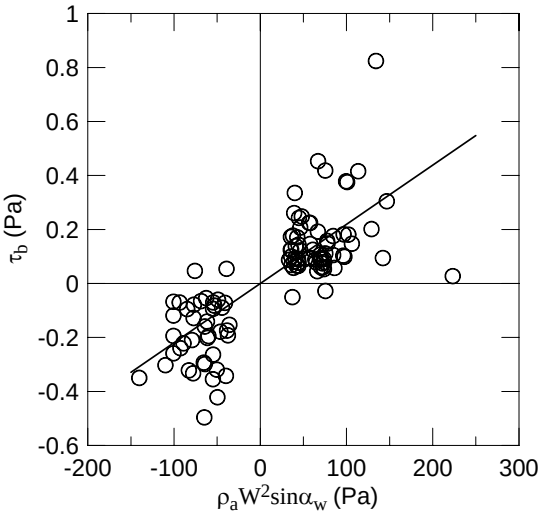

Figure 12 Relationship between τ_b and $\rho_a W^2 \sin\alpha_w$. The solid line is the regression line obtained with the method of the least squares.

another nonlinear formula of the bottom friction stress proposed by *Thornton and Guza* [1986], which is 0.006 ± 0.0007; the formula in *Thornton and Guza* [1986] becomes Eq.(4) when the wave angle is equal to zero.

The wind stress was estimated using

$$\tau_s = C_d \rho_a W^2 \sin\alpha_w, \qquad (6)$$

where C_d is a nondimensional coefficient, ρ_a is the air density, W is the wind velocity and α_w is the wind angle. The coefficient C_d was estimated with $\tau_b = \tau_s$, which is the momentum balance equation when the wave height is small and the cross-shore gradient of the radiation stress is assumed to be negligible. The data at P380m obtained when the deepwater wave height was smaller than 1.0 m and the absolute value of the alongshore component of the wind velocity was larger than 5.0 m were used for the estimation of C_d. The coefficient C_d estimated with the least square method is 0.0022 (r = 0.60, **Figure 12**), which is within the range of the previously obtained C_d, from 0.001 to 0.0025 [*Geernaert et al.*, 1986].

The cross-shore gradients of the radiation stresses at the measurement points were estimated from $dS_{yx}/dy = \tau_b - \tau_s$. Errors of dS_{yx}/dy were estimated on the basis of the root-mean-square error of the wave height, 30%.

The averaged values of the cross-shore gradient of the radiation stress and the averaged wind stress are almost

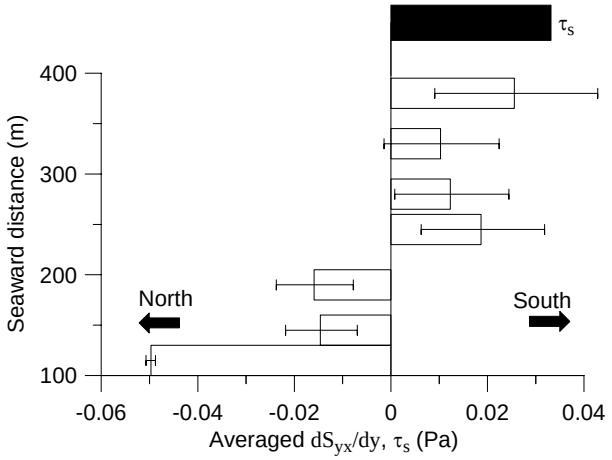

Figure 13 Averaged values of τ_s (black) and dS_{yx}/dy (white). The horizontal lines show the error ranges.

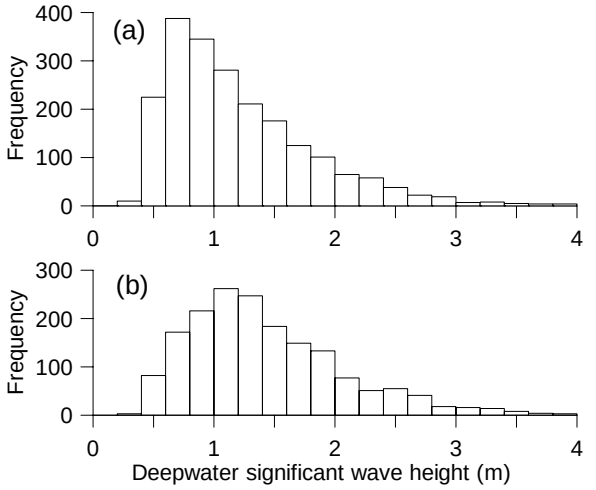

Figure 14 Frequency distribution of deepwater significant wave height when the longshore current direction at P115m was northward (a) and southward (b).

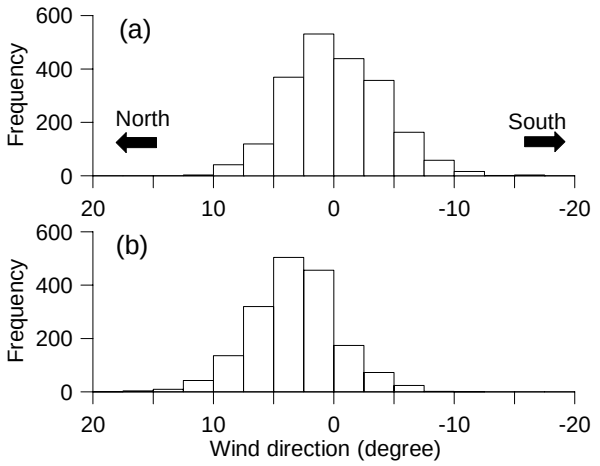

Figure 15 Frequency distribution of wind direction when the longshore current direction at P115m was northward (a) and southward (b). The wind direction from the north is defined as being positive.

comparable (**Figure 13**). The result that the contribution of the wind on the longshore current velocity is not negligible even in the nearshore zone is consistent with previous studies [*Larson and Kraus*, 1991; *Whitford and Thornton*, 1993].

Because the cross-shore gradient of the radiation stress and the wind stress have comparable contributions on the long-term average longshore current velocity, the causes of the cross-shore variation of long-term average longshore current velocity were investigated using the wave and wind data.

3.3 Causes of cross-shore variation of long-term average longshore current

The frequency distributions of the deepwater significant wave height when the northward and southward longshore currents developed at P115m show that the deepwater wave height with the northward current is smaller than that with the southward current (**Figure 14**). As for wind, the frequency of the wind from the north is almost equal to that from the south when the northward current developed, whereas the frequency of the wind from the north is much larger than that from the south when the southward current developed (**Figure 15**).

When the northward longshore current developed near the shore, the waves broke near the shore, and the width of the surf zone, where the longshore current developed, was narrow because the deepwater wave height was relatively small. Since the frequency of the wind from the north was almost equal to that from the south, the longshore current velocity averaged during the measurement period outside the surf zone, where the longshore current is mainly caused by wind, became close to zero. As a result, the northward longshore current developed near the shore, but decreased to zero outside the relatively narrow surf zone.

On the other hand, when the southward longshore current developed near the shore, the waves broke far from the shore and the surf zone was wider because the deepwater wave height was relatively large. Furthermore, the southward longshore current developed even outside the surf zone because the wind from the north was predominant. As a result, a southward longshore current velocity with relatively

uniform cross-shore variation developed.

The properties of the two cross-shore variations are consistent with those shown in **Figure 10**. The superposition of the two variations produced a cross-shore variation of long-term average longshore current velocity with northward velocity near the shore and southward velocity far from the shore.

4. Discussion

The long-term average longshore current velocities shown in **Figure 9** contain errors caused by the measurement method with the float and discrete measurement periods and points.

The error caused by the float measurement is estimated from the difference between the longshore current velocity measured with the float and that with the electro-magnetic current meter, which is assumed to be the true current velocity. Because the standard deviation of the difference σ is 0.086 m/s as mentioned in **2.**, the error caused by the float measurement, which is estimated with the standard deviation σ and the total data number *n*, 5473, as $\sigma / \sqrt{n}$, is 0.0012 m/s.

The time interval of the measurement, one day, may cause another error in the long-term average longshore current velocity because the longshore current velocity varies according to the tide as shown in *Thornton and Kim* [1993]. We investigated the influence of the tide on the longshore current velocity at Hasaki using a 1-D model for longshore current velocity under irregular waves [*Kuriyama and Nakatsukasa*, 2000]. The validity of the model was confirmed with longshore current velocities measured at Hasaki and other coasts [*Kuriyama and Nakatsukasa*, 2000].

The longshore current velocities under the high, mean and low tides were estimated with the mean deepwater wave height and period (1.34 m and 7.97 s) and the mean beach profile in the measurement period (**Figure 4**). The seaward boundary was set at P925m as in **3.2**, and the deepwater wave angle was set to be 13.1 degrees, which is based on the average of the absolute value of the wave angle visually observed at the tip of the pier.

The estimated longshore current velocities are shown in Figure 16. The current velocities shoreward of P200m are comparable to or larger than the long-term average longshore current velocities when the northward and southward currents developed at P115m (**Figure 10**). This result suggests that the

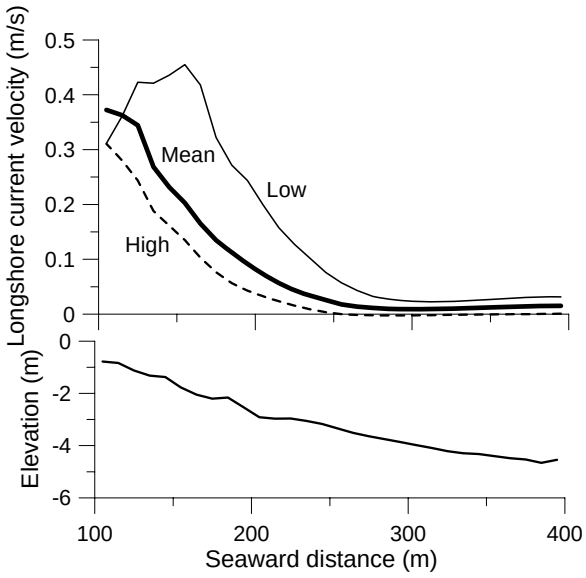

Figure 16 (a) Longshore current velocities estimated with mean wave height, period and direction under the high (thin solid line), mean (thick solid line) and low tides (broken line), and (b) mean beach profile.

longshore current velocities shoreward of P200m estimated with the mean wave height, period and direction are appropriate for estimation of the error due to tide in the long-term average longshore current velocity.

The differences between the estimated longshore current velocities at the high and mean tides ΔU_1, and those between the velocities at the low and mean tides ΔU_2 were estimated, and the maximum value of $\left(\left|\Delta U_1\right| + \left|\Delta U_2\right|\right)/2$ along the pier was taken as the error due to tide in a measurement, which is the difference between the longshore current velocities measured once a day and averaged over a day. The maximum value is 0.16 m/s, which takes place at P155m, and on the basis of the value, the error caused by tide in the long-term average longshore current velocity is estimated to be 0.0022 m/s ($=0.16/\sqrt{5473}$).

The vertical variations of the longshore current velocities were not measured in the present study, leading to another source of error. The influence of the vertical variation on the long-term average longshore current velocity was investigated in the following manner. First, the logarithmic vertical variation was assumed as shown by Eq. (7).

$$u(z) = \frac{u_*}{\kappa} \ln(\frac{z}{z_a}), \qquad (7)$$

where u(z) is the longshore current velocity at z, z is positive upward from the bottom, u_* is the alongshore shear stress velocity, κ is the Von Karman constant (0.4), and z_a is the apparent roughness height. With Eq. (7) and the long-term average longshore current velocities, which were estimated on the basis of the data obtained 1 m below the surface, the vertically averaged values of the long-term average longshore current velocities were estimated. In the estimation, the roughness height was set at 5.0 cm, which is close to the maximum value of z_a shown in *Garcez-Faria et al.* [1998], and the mean tide and the mean beach profile were used.

The long-term average longshore current velocities and the values vertically averaged with Eq. (7) are shown in **Figure 17** as well as the sum of the errors caused by the float measurement and tide, 0.0034 m/s.

The overall errors, which are caused by the float measurement, tide and the vertical current profile, are relatively small compared with the long-term average longshore current velocities. Furthermore, the direction of the long-term average longshore current velocity near the shore is consistent with the direction of the predominant longshore sediment transport estimated on the basis of the shoreline changes [*Sato and Tanaka*, 1966]. These results confirm the conclusion that the long-term average longshore current velocity is to the north near the shore, but to the south away from the shore.

Kraus and Sasaki [1979] showed that the cross-shore variation of the longshore current velocity with a large incident wave angle has a peak velocity closer to the shore and smaller velocities outside the surf zone than that with a small wave angle. Although we do not have accurate data for wave angle as mentioned in **3.3**, the absolute value of the averaged wave angle visually observed at the tip of the pier when the southward longshore currents developed at P115m is 8.6 degrees and slightly larger than that with the northward currents, 6.1 degrees. The difference in the wave angle produces a difference in the longshore current velocity such that the cross-shore variation of the southward longshore current has a peak closer to the shore and lesser velocity outside the surf zone than that of the northward current. The difference is contrary to that obtained from the field data as shown in **Figure 10**. Hence, it is unlikely that the difference in the wave angle when the southward and northward longshore currents developed has a strong influence on the cross-shore variation of the long-term average longshore current velocity.

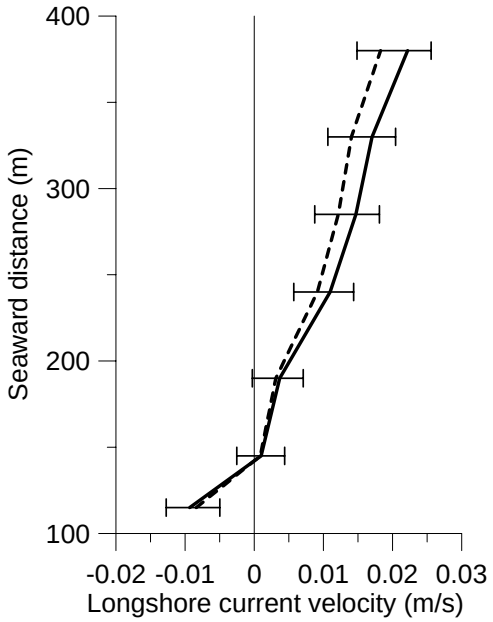

Figure 17 Cross-shore variations of the long-term average longshore current velocities U (solid line) and vertically averaged values with Eq. (7) U_v (broken line). The error bars (horizontal thin lines) show the ranges of $U_a \pm (\varepsilon_1 + \varepsilon_2)$, where U_a=(U+U_v)/2, ε_1=(U- U_v)/2 and ε_2 is the error caused by the float measurement and tide, 0.0034 m/s.

There is another possibility that the seasonal variation of the beach profile has an influence on the long-term average longshore current velocity, and hence the influence was numerically investigated using the 1-D model for longshore current velocity [*Kuriyama and Nakatsukasa*, 2000] with the averaged deepwater wave dimensions and the mean beach profiles in summer and winter seasons. Here, the summer and winter seasons were determined on the basis of the seasonal variation of the wave angle (**Figure 6**) and the summer season was set as being from April to September, when waves came from the south, and the winter season from October to March, when waves came from the north.

The difference of the cross-shore variations of the estimated longshore current velocities is small as shown in Figure 18. Furthermore, the variation in the winter season, when the southward current is predominant, has a peak

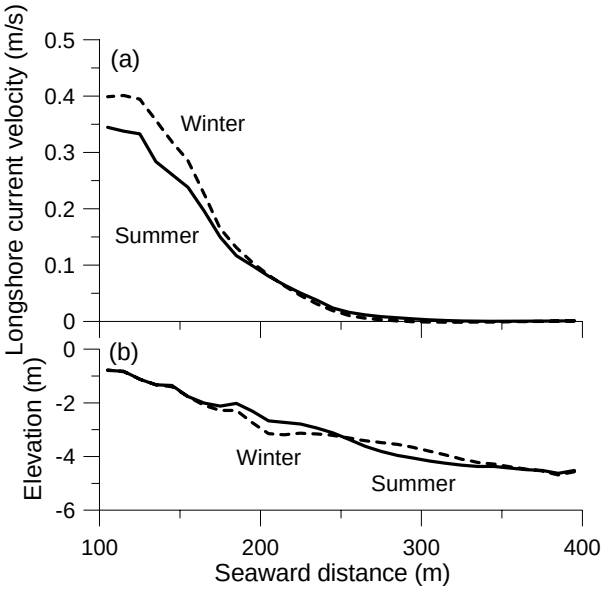

Figure 18 Longshore current velocities estimated with mean wave height, period and direction in summer (solid line) and winter (broken line) seasons (a), and the mean beach profiles in summer (solid line) and winter (broken line) seasons (b).

velocity slightly closer to the shore than that in the summer season, when the northward current is predominant. This is contrary to the measurement findings. Hence, the influence of the seasonal beach profile change on the long-term average longshore current velocity is assumed to be small.

The possibility that the direction of the predominant longshore sediment transport near the shore differs from that far from the shore is suggested by a previous study on morphological changes around a port [*Sato*, 1996]. The conclusions of this study demonstrate that cross-shore variation of the long-term average longshore current velocity in opposite directions near and away from the shore is likely to occur under the conditions where the wave height and the wind angle when waves come from one side are different from those when waves come from the other side. The conclusions suggest that even in the nearshore zone, the direction of net longshore sediment transport far from the shore may be the opposite to that near the shore. If so on an eroded beach on the downdrift side of a coastal structure, a strong candidate for the borrow site is the offshore, where accretion is expected to take place owing to the net longshore sediment transport opposite to that near the shore.

Although this study investigated the long-term average longshore current velocity, there were temporal variations in the longshore current velocity as shown in **Figure 9**. The cumulative longshore current velocity shifted to the north from 1994 to 2000 in particular near the shore, which indicates that the northward current velocity was larger during the period than during the other periods. The variations will be investigated in future studies.

5. Conclusions

Longshore Longshore current velocities were measured once a day at intervals of about 50 m along the 427-meter-long pier during a 15-year period from 1987 to 2001. The results show that the direction of the long-term average longshore current velocity away (> 200 m) from the shore was the opposite to that near the shore; the southward current was dominant offshore, whereas the northward current was near the shore.

The cross-shore variation of the long-term average longshore current velocity was formed owing to the difference between the wave and wind conditions when the northward and southward longshore currents developed. When the northward current developed, the deepwater wave height was relatively small and the frequency of the wind from the north was almost equal to that from the south. Consequently, the northward current developed only near the shore, in the narrow surf zone; outside the surf zone, the northward current velocity decreased to zero. On the other hand, when the southward current developed, the deepwater wave height was relatively large and the wind from the north was predominant. Hence, the southward longshore current developed not only in the wide surf zone but also outside the surf zone, and the cross-shore variation of the longshore current velocity became relatively uniform. The superposition of the two cross-shore variations produced the cross-shore variation of the long-term average longshore current velocity with a northward velocity near the shore and a southward velocity far from the shore. The conclusions suggest that the direction of net longshore sediment transport offshore may be the opposite to that near the shore.

(*Received on August 4, 2006*)

Acknowledgements

The offshore data were provided by Kashima Port Construction Office of Ministry of Land, Infrastructure and

Transport, and Marine Information Division of Port and Airport Research Institute. We thank all the staff members at Hazaki Oceanographical Research Station (HORS) who conducted the field measurements even during violent typhoons.

References

Church, J. C. and E. B. Thornton (1993), Effects of breaking wave induced turbulence within a longshore current model, *Coastal Eng., 20*, 1-28.

Garcez-Faria, A. F., E. B. Thornton, T. P. Stanton, C. V. Soares, and T. C. Lippmann (1998), Vertical profiles of longshore currents and related bed shear stress and bottom roughness, *J. Geophysical Research, 103*(C2), 3217-3232.

Geernaert, G. L., K. B. Katsaros, and K. Richter (1986), Variation of the drag coefficient and its dependence on sea state, *J. Geophysical Research, 91*(C6), 7667-7679.

Goda, Y. and N. Watanabe (1991), A longshore current formula for random breaking waves, *Coastal Eng. in Japan, 34*(2), 159-175.

Hamilton, D. G. and B. A. Ebersole (2001), Establishing uniform longshore currents in a large-scale sediment transport facility, *Coastal Eng., 42*, 199-218.

Hashimoto, N., K. Kawaguchi, T. Maki, and T. Nagai (2000): A comparison of WAM and MRI based on observed directional wave spectra, in *Hydrodynamics IV*, Vol. II, edited by Y. Goda et al., pp.587-592, ICHD2000 Local Organizing Committee, Yokohama, Japan.

Horikawa, K. (1978): *Coastal Engineering, An Introduction of Ocean Engineering*, 402pp., University of Tokyo Press, Tokyo, Japan.

Komar, P. D. (1998): *Beach Processes and Sedimentation, Second Edition*, 544pp., Prentice-Hall, New Jersey.

Kraus and Sasaki (1979): Influence of wave angle and lateral mixing on the longshore current, *Marine Science Communications, 5*(2), 91-126.

Kuriyama, Y. (1991): Investigation on cross-shore sediment transport rates and flow parameters in the surf zone using field data, in *Report of the Port and Harbour Research Institute*, Vol. 31(2), pp.3-58, Port and Harbour Res. Inst., Yokosuka, Japan.

Kuriyama, Y. (1995), Longshore current on a bar-tough beach –Field investigation and verification of numerical models, *Bull. Permanent Int. Assoc. Navigation Cong., 86*, 79-94.

Kuriyama, Y. (1998): Field measurements of undertow on longshore bars, in *Proceedings of the 26th International Conference on Coastal Engineering*, pp.297-310, Am. Soc. Civil. Eng., New York.

Kuriyama, Y. and Y. Ozaki (1993), Longshore current distribution on a bar-trough beach –Field measurements at HORF and numerical model-, in *Report of the Port and Harbour Research Institute*, Vol. 32(3), pp.3-37, Port and Harbour Res. Inst., Yokosuka, Japan.

Kuriyama, Y. and T. Nakatsukasa (2000), A one-dimensional model for undertow and longshore current on a barred beach, *Coastal Eng., 40*, 39-58.

Kuriyama, Y. (2002), Medium-term bar behavior and associated sediment transport at Hasaki, Japan, *J. Geophys. Res., 107*(C9), 3132, doi:10.1029/2001JC000899.

Larson, M. and N. C. Kraus (2001), Numerical model of longshore current for mar and trough beaches, *J. Waterway, Port, Coastal, and Ocean Eng., 117*, 326-347.

Longuet-Higgins, M. S. (1970a): Longshore currents generated by obliquely incident waves, 1, *J. Geophys. Res., 75*, 6778-6789.

Longuet-Higgins, M. S. (1970b): Longshore currents generated by obliquely incident waves, 2, *J. Geophys. Res., 75*, 6790-6801.

Nishimura, H. (1988): Computation of nearshore current, in *Nearshore Dynamics and Coastal Process –Theory, Measurements and Predictive Models-*, edited by K. Horikawa, pp.271-291, University of Tokyo Press, Tokyo, Japan.

Reniers, A. J. H. M. and J. A. Battjes (1997), A laboratory study of longshore currents over barred and non-barred beaches, *Coastal Eng., 30*, 1-22.

Ruessink B. G., J. R. Miles, F. Feddersen, R. T. Guza, and S. Elgar (2001), Modeling the alongshore current on barred beaches, *J. Geophys. Res., 106*(C10), 22,451-22,463.

Sato, S. and N. Tanaka (1966): Field investigation on sand drift at Kashima facing the Pacific Ocean, in *Proceedings of the 10th International Conference on Coastal Engineering*, pp.595-614, Am. Soc. Civil. Eng., New York.

Sato, S. (1996), Effects of winds and breaking waves on large-scale coastal currents developed by winter storms in Japan Sea, *Coastal Eng. in Japan, 39*(2), 129-144.

Smith, J. M., M. Larson, and N. C. Kraus (1993), Longshore current on a barred beach: Field measurements and calculation, *J. Geophys. Res., 98*(C12), 22,717-22,731.

Thornton, E. B. and R. T. Guza (1986), Surf zone longshore

currents and random waves: field data and models, *J. Physical Oceanography*, *16*, 1165-1178.

Thornton, E. B. and C. S. Kim (1993), Longshore current and wave height modulation at tidal frequency inside the surf zone, *J. Geophysical Research*, *98*(C9), 16,509-16,519.

Visser, P. J. (1984): Uniform longshore current measurements and calculations, in *Proceedings of the 19th International Conference on Coastal Engineering*, pp. 2192-2207, Am. Soc. Civil. Eng., New York.

Whitford, D. J. and E. B. Thornton (1993), Comparison of wind and wave forcing of longshore currents, *Continental Shelf Research*, *13*(11), 1205-1218.

CONTENTS

1. Medium-Term Variations of Bar Properties and Their Linkages with Environmental Factors at HORS
……Yoshiaki KURIYAMA, Shin-ichi YANAGISHIMA……1

2. Cross-shore Variation of Long-Term Average Longshore Current Velocity at HORS
…… Yoshiaki KURIYAMA, Shin-ichi YANAGISHIMA……15

3. Adsorption Characteristics of Organotin Compounds onto Parts and Harbors Sediments
Yoshiyuki NAKAMURA, Tomohiro YAMASAKI, Susumu KONUMA, Akira KAGAYAMA, Shigeki MASUNAGA……31

4. The Role of Suction in Tidal Flat Geoenvironments and Burrowing Activity of Benthos
-Parformance Index for Conservation and Restoration of Intertidal Sandy Flats-
……Shinji SASSA, Yoichi WATABE……61